UDK 66.087:669.24:669.058.6
Original scientific article/Izvirni znanstveni članek

ISSN 1580-2949
MTAEC9, 53(5)687(2019)

EVOLUTION IN ELECTROCHEMICAL PERFORMANCE OF $Co(OH)_2$ ELECTRODEPOSITED ON NICKEL FOAM AS HIGH-PERFORMANCE SUPERCAPACITORS WITH APPLIED POTENTIAL AND $Co(NO_3)_2$ CONCENTRATION

RAZVOJ ELEKTRO-KEMIČNIH LASTNOSTI ELEKTRIČNO NANEŠENEGA $Co(OH)_2$ NA NIKLJEVO PENO Z UPORABO ELEKTRIČNEGA POTENCIALA IN KONCENTRACIJE $Co(NO_3)_2$ KOT VISOKOKVALITETNEGA SUPER-KONDENZATORJA

Zhongjie Lu, Jun Li*, Wanli Jia, Yunqiang Jiang, Yongfei Juan

School of Materials Engineering, Shanghai University of Engineering Science, Shanghai, 201620, China

Prejem rokopisa – received: 2018-12-26; sprejem za objavo – accepted for publication: 2019-04-11

doi:10.17222/mit.2018.276

$Co(OH)_2$/NF electrodes with a high specific capacitance and an excellent cyclic stability were successfully prepared by directly electrodepositing $Co(OH)_2$ on nickel foam (NF). The synthesis and nucleation mechanisms of $Co(OH)_2$ were revealed. The evolution in morphology and electrochemical performance with deposited potential and $Co(NO_3)_2$ concentration were investigated. The mechanism in terms of the increase in specific capacitance after 1000 cycles was explored. The results indicated that $Co(OH)_2$ was nucleated by instantaneous nucleation, and deposited by a single electrochemical reaction $NO_3^- + 7H_2O + 8e^- \rightarrow NH_4^+ + 10OH^-$ followed by a chemical reaction $Co^{2+} + 2OH^- \rightarrow Co(OH)^2$. A high potential accompanied with a high $Co(NO_3)_2$ concentration accelerated the growth of the $Co(OH)_2$, causing a decrease in the specific surface area of $Co(OH)_2$. The highest specific surface area was obtained in the $Co(OH)_2$/NF electrode prepared at –0.65 V in a 0.1 mol·L^{-1} $Co(NO_3)_2$ solution, at which a highest specific capacitance was measured by CV (836 F·g^{-1}) and galvanostatic charge/discharge (725 F·g^{-1}). Its specific capacitance was drastically increased from 836 to 1116 F·g^{-1} when it was immersed into a KOH solution and underwent 1000 cycles, which resulted from the removal of the incorporated $Co(NO_3)_2$ into the active substances (increasing the active sites) and the transformation of the α-$Co(OH)_2$ to β-$Co(OH)_2$ (enhancing the electrode conductivity).

Keywords: electrochemical deposition, β-$Co(OH)_2$, nucleation mechanisms, potential, concentration, supercapacitors

Avtorji v prispevku opisujejo uspešno sintezo $Co(OH)_2$/NF elektrod z visoko specifično kapaciteto in odlično ciklično stabilnostjo. Le-to so izvedli z direktnim električnim nanosom oz. depozicijo $Co(OH)_2$ na nikljevo peno (NF). Razvili so sintezo in odkrili mehanizme nukleacije oz. tvorbe kali $Co(OH)_2$. Raziskali so njen razvoj in morfologijo nanosa ter njene elektrokemijske lastnosti z depozicijskim potencialom in koncentracijo $Co(NO_3)_2$. Učinke povečanja specifične kapacitete so raziskovali po 1000 ciklih. Rezultati kažejo, da se je nukleacija $Co(OH)_2$ zgodila s t.i. spontano nukleacijo in da je do depozicije prišlo z naslednjo elektrokemično reakcijo: $NO_3^- + 7H_2O + 8e^- \rightarrow NH_4^+ + 10OH^-$, kateri je sledila kemična reakcija $Co^{2+} + 2OH^- \rightarrow Co(OH)^2$. Visok potencial, združen z visoko koncentracijo $Co(NO_3)_2$ je pospešil rast $Co(OH)_2$, kar je zmanjšalo presek specifične površine $Co(OH)_2$. Le-ta je bil največji pri elektrodi $Co(OH)_2$/NF, pripravljeni pri –0.65 V in v raztopini 0.1 mol·L^{-1} $Co(NO_3)_2$. Pri teh pogojih so izmerili najvišjo specifično kapaciteto nanosa (836 F·g^{-1}) s ciklično voltametrijo (CV) in galvanostatično naelektritev/razelektritev (725 F·g^{-1}). Njegova specifična kapaciteta je drastično narasla z 836 F·g^{-1} na 1116 F·g^{-1}, ko je bil potopljen v raztopino KOH in izpostavljen 1000 ciklom, kar je povzročilo spremembo vgrajenega $Co(NO_3)_2$ v aktivno substanco, zaradi povečanja aktivnih položajev, in pretvorbo α-$Co(OH)_2$ v β-$Co(OH)_2$ (povečanje prevodnosti elektrode).

Ključne besede: elektrokemična depozicija, β-$Co(OH)_2$, mehanizmi nukleacije, potencial, koncentracija, superkondenzatorji

1 INTRODUCTION

The shortage of energy and the environmental pollution are increasingly serious, which is accelerating the development of renewable and clean energy conversion and storage systems. Supercapacitors, as a new type of energy-storage device that can make up for the traditional storage devices in the energy/power density, have attracted considerable attention.[1,2] The electrode material is regarded as a decisive factor responsible for the electrochemical performance of supercapacitors. Cobalt hydroxide ($Co(OH)_2$) has become a research hot spot due to its high theoretical specific capacitance of up to 3460 F·g^{-1}, controllable layer spacing/layered structure and high electrochemical reaction activity.[3–8] A large number of investigations into the synthesis of $Co(OH)_2$ electrode by different methods (such as the hydrothermal method,[4,7,9] chemical deposition method,[7] vapor deposition process[11] and electrochemical deposition[11–13]) have been carried out. L. B. Kong et al.[4] synthesized $Co(OH)_2$ nanoflakes by the hydrothermal method with cobalt chloride hydrate solution and NaOH as the reactants. $Co(OH)_2$ powder (80 %) was mixed with acetylene black (7.5 %), conducting graphite (7.5 %) and tetrafluoro-

*Corresponding author's e-mail:
jacob_lijun@sues.edu.cn

ethylene (5 %). The electrode was fabricated by pressing the resulting paste on a nickel gauze with a load of 10 MPa. The specific capacitance and specific energy of the electrode reached 72.4 $F \cdot g^{-1}$ and 92.7 $Wh \cdot kg^{-1}$ within the potential range of 0–1.6 V, respectively. It demonstrated a good cycling performance with a capacitance attenuation of 6.8 % over 1000 cycles. Y. F. Tang et al.[6] synthesized monodispersed β-$Co(OH)_2$ nanowires by a facile hydrothermal process with a hexadecyltrimethyl ammonium bromide (CTAB) as a soft template, the morphology and size of which were controlled by regulating the CTAB content and the reaction time. Then, 80 % b-$Co(OH)_2$ nanowires, 15 % acetylene black and 5 % polyvinylidene difluoride (PVDF) were mixed in the ethanol to form a homogeneous slurry. The slurry was coated on the pre-cleaned Pt meshwork and dried in vacuum at 80 °C to obtain the electrode. The results of the electrochemical tests indicated that the specific capacitance of the electrode was 358 $F \cdot g^{-1}$ at a current density of 0.5 $A \cdot g^{-1}$. J. P. Cheng et al.[14] prepared the $Co(OH)_2$ electrode by pressing a mixture of $Co(OH)_2$ prepared by the hydrothermal method, acetylene black and polyvinylidene fluoride (PVDF) in the weight ratio of 8:1:1. Its specific capacitance reached 153 $F \cdot g^{-1}$ at a scanning rate of 5 $mV \cdot s^{-1}$. Z. A. Hu et al.[15] synthesized the four α-$Co(OH)_2$ powders with different anions salts ($CoCl_2 \cdot 6H_2O$, $Co(NO_3)_2 \cdot 6H_2O$, $CoSO_4 \cdot 7H_2O$, and $Co(CH_3COO)_2 \cdot 4H_2O$), polyethylene glycol and $NH_3 \cdot H_2O$ by a chemical precipitation route. The electrodes were also prepared by pressing mixtures containing as-prepared powder, acetylene black, conducting graphite and polytetrafluoroethylene (PTFE) binder (75:10:10:5 in weight ratio) onto a nickel foam. The specific capacitances of the samples with intercalated anion chloride, nitrate, acetate, and sulfate were (697, 638, 526, and 420) $F \cdot g^{-1}$, respectively.

Up to now, $Co(OH)_2$ is mainly synthesized in the form of a powder, which cannot be used directly as electrodes. The preparation of the electrode usually includes three processes, corresponding to the synthesis of $Co(OH)_2$ powder, the mixing of $Co(OH)_2$, conductive materials (carbon black or acetylene black) and binders (polytetrafluoroethylene, polyvinylidene fluoride) in certain proportions, electrode assembly.[4,6,12,15]. The whole route is comparatively complicated, which can result in the low reproducibility of the electrode performance. Moreover, the electrode conductivity is weakened, resulting from the additives. The electrodeposition method can effectively solve the above shortcomings, by which the electrode can be directly prepared by depositing the active substances on different substrates. Moreover, its precise controllability, ease of operation, high deposition rate, good repeatability and low cost also accelerate its application in the electrode preparation. Deng et al[13] synthesized $Co(OH)_2$ petal nanometer flakes in a $Co(NO_3)_2$ solution by electrochemical deposition with carbon-fiber paper (CFP) as the base. Then, a-$Co(OH)_2$ was transformed into b-$Co(OH)_2$ in the KOH solution. The specific capacitance measured was 800 $F \cdot g^{-1}$ at a current density of 2 $A \cdot g^{-1}$, and 95.7 % of the initial value was remained after 8000 cycles. C. M. Zhao et al.[16] deposited graphene on foamed nickel by plasma vapor deposition, and then electrodeposited $Co(OH)_2$ nanosheets on the graphene/foamed nickel substrate in an aqueous solution containing 0.1 $mol \cdot L^{-1}$ $Co(NO_3)_2$. The specific capacitance of the composite electrode material was 693.8 $F \cdot g^{-1}$ at a current density of 2 $A \cdot g^{-1}$. At the same time, the residual capacitance of the electrode was 91.9 % after 3000 cycles of charge and discharge under a high current density of 40 $A \cdot g^{-1}$. M. Li et al.[17] firstly synthesized the precursors of Ni/Si–MCPs by electrodepositing Ni on silicon microchannel plates (MCPs) in the solution of $NiCl_2 \cdot 6H_2O$ and H_3BO_3, then further prepared the $Co(OH)_2$/Ni/Si-MCPs electrode by continuous electrochemical deposition in the $Co(NO_3)_2 \cdot 6H_2O$ solution. The electrode exhibited a specific capacitance of 697.56 $F \cdot g^{-1}$ at a current density of 2 $mA \cdot cm^{-2}$ and a retention rate of 91.20 % after 2500 cycles.

It is well known that the electrochemical performance of an electrode is closely related to its morphology and structure when the electrode material is determined.[13,18] The morphology and structure of the electrode material prepared by electrochemical deposition mainly depend on the deposition potential[21], temperature[19,20], time[21] and electrolyte.[15] At present, research mainly focuses on the electrochemical performance of the electrode produced under the fixed conditions, or its change resulting from the variation in a certain factor. There are few reports about the effect of the interaction between the two even more factors on the electrochemical performance. Moreover, the electrodeposition mechanism of $Co(OH)_2$ is less studied.

In this study, $Co(OH)_2$ was electrodeposited on nickel foam to form the electrodes in the solution containing $NaNO_3$ and $Co(NO_3)_2$. The deposited process/nucleation mechanisms of $Co(OH)_2$ were revealed. The evolution in morphology of $Co(OH)_2$ with the change in applied potential –0.60 V, –0.65 V, –0.70 V, –0.75 V, –0.80 V, –0.85 V, –0.90 V, –0.95 V and $Co(NO_3)_2$ concentration (0.1 $mol \cdot L^{-1}$, 0.9 $mol \cdot L^{-1}$) was investigated in detail. The electrochemical performance of those electrodes deposited at different potentials/$Co(NO_3)_2$ concentrations were evaluated by means of cyclic voltammetry (CV) and galvanostatic charge/discharge methods. Finally, the suitable potential and $Co(NO_3)_2$ concentration were confirmed, at which the electrode exhibited a high specific capacitance and an excellent cycling stability. In particular, the mechanism about the increase in specific capacitance of the electrode after 1000 cycles was explored in depth.

2 EXPERIMENTAL PART

2.1 The synthesis/nucleation mechanisms of $Co(OH)_2$

Cobalt nitrate [$Co(NO_3)_2.6H_2O$] (Sinopharm Chemical Reagent Co., Ltd) and sodium nitrate ($NaNO_3$) (Shanghai Titan Scientific Co., Ltd) with analytical grade were selected to prepare two aqueous solutions containing 0.075 mol·L^{-1} $NaNO_3$ and 0.1 mol·L^{-1}/0.9 mol·L^{-1} $Co(NO_3)_2$. The investigations were carried out on an electrochemical workstation system (CHI 6082D, CH Instruments Ins, Shanghai, China) with a conventional three-electrode system at room temperature. Nickel foam with a size of 20 mm × 20 mm × 0.5 mm (Shanxi Power Source Battery Materials Co., Ltd., Taiyuan, Shanxi, China) and graphite with a size of 25 mm × 20 mm × 1 mm (Beijing Electrical Carbon Factory, Beijing, China) were used as the working electrode and counter electrode, respectively. They were degreased with an acetone solution in an ultrasonic bath, and then treated in 1 mol·L^{-1} HCl solution and deionized water for 10 min at room temperature in turn. Then, the two electrodes with a height of 10 mm were immersed into the solutions, between which a 10 mm distance was controlled. A saturated calomel electrode (SCE) was selected as the reference electrode.

The synthesis process of $Co(OH)_2$ was investigated by the cyclic voltammetry (CV) test. The potential was swept from 0 V to –1 V, and increased to 0 V at a scanning rate of 5 mV·s^{-1}. The nucleation mechanism of $Co(OH)_2$ was revealed by the chrono-amperometry test with the applied potentials of –0.60 V, –0.65 V, –0.70 V and –0.80 V and –0.95 V for 30 min.

2.2 The electrodeposition of $Co(OH)_2$

The electrodeposition of $Co(OH)_2$ was carried out in the two solutions with 0.075 mol·L^{-1} $NaNO_3$ and 0.1 mol·L^{-1} /0.9 mol·L^{-1} $Co(NO_3)_2$. Different potentials (vs. SCE: –0.60 V, –0.65 V, –0.70 V, –0.75 V, –0.80 V, –0.85 V, –0.90 V and –0.95 V) were applied for the electrodeposition with a time of 30 min. Prior to the deposition, nickel foam was dried at room temperature, then weighed using a Sartorius SQP electronic balance (0.01 mg, Sartorius, Beijing, China). After the deposition, the nickel form covered with $Co(OH)_2$ was washed three times in succession in deionized water for 10 min. Then, it was dried at room temperature, and weighed again to obtain the weight of the deposit by subtracting the weight of nickel foam.

2.3 The tests for electrochemical performance of $Co(OH)_2$ electrodes

The electrochemical performance of the $Co(OH)_2$ electrodes was evaluated by CV and galvanostatic charge/discharge tests. A 2 mol·L^{-1} KOH aqueous solution was selected as the supporting electrolyte. The scanning potential of the CV was ranged from –0.2 V to 0.5 V at a scanning rate of 5 mV·s^{-1}. Galvanostatic charge/discharge was performed in the potential range of –0.1 V to 0.45 V at a current density of 4 A·g^{-1}.

2.4 The characterization of deposited $Co(OH)_2$

Prior to the electrochemical tests, the evolution in morphology of the deposits prepared at the applied potentials of –0.60 V/–0.65 V/–0.95 V in the solutions with 0.1 mol·L^{-1} and 0.9 mol·L^{-1} $Co(NO_3)_2$ was investigated in detail by a HITACHI S-4800 scanning electron microscope (SEM, Hitachi Limited, Tokyo, Japan). After the electrochemical tests, the morphology of the deposit prepared at –0.65 V in the solution with 0.1 mol·L^{-1} $Co(NO_3)_2$ was checked again by SEM. Before and after the electrochemical tests, the changes in the chemical state of the Co in the deposit prepared at –0.65 V in the solution with 0.1 mol·L^{-1} $Co(NO_3)_2$ were identified by an X-ray photo-electron spectroscope (XPS; ESCALAB 250Xi, Thermo Fisher Scientific, Massachusetts, USA). The narrow-scan spectra were acquired with a Kratos Axis Ultra spectrometer using a monochromatic Al–K_α source. The energy step of 0.1 eV was selected for the spectra. The binding-energy scale was calibrated according to the C_{1s} peak (at 781 eV) for the adventitious Co on the analyzed sample surface. The lattice fringes of the deposits for the XPS analyses were obtained by a transmission electron microscope (TEM; JEM-2100F, JEOL, Tokyo, Japan).

3 RESULTS AND DISCUSSION

3.1 The synthesis/nucleation mechanisms of $Co(OH)_2$

Figure 1 indicates the cyclic voltammogram (CV) curves recorded on nickel foam in a solution consisting of 0.1 mol·L^{-1} $Co(NO_3)_2$ at a scanning rate of 5 mV·s^{-1}. When the potential is higher than –0.60 V during the negative-going scan, the current approximately tends to zero, indicating that almost no ions participate in the electrode reactions. However, the current is rapidly enhanced to about 0.035 A with the potential decreased

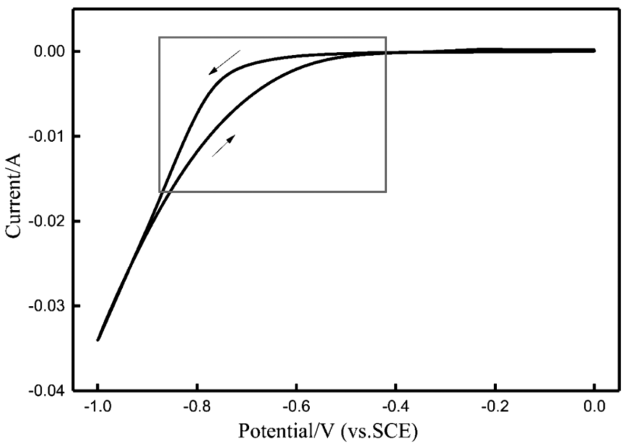

Figure 1: CV curves recorded on nickel foam in a solution consisting of 0.1 mol·L^{-1} $Co(NO_3)_2$ at a scanning rate of 5 mV·s^{-1}

from –0.60 V to –1.0 V. An obvious inflexion can be observed clearly at about –0.65 V (as marked with a rectangle), indicating that $Co(OH)_2$ is synthesized by a one-step electrochemical reaction at about –0.65 V.[17] The synthesis process may include two reactions, corresponding to an electrochemical reaction and a chemical deposition reaction in Equations (1) and (2):[22,23]

$$NO_3– + 7H_2O + 8e^- \rightarrow NH_4^+ + 10OH^- \quad (1)$$

$$Co^{2+} + 2OH– \rightarrow Co(OH)^2 \quad (2)$$

Chrono-amperometry was further applied to explore the nucleation mechanism of $Co(OH)_2$ at five different potentials (–0.60 V, -0.65 V, –0.70 V, –0.80 V, –0.95 V). As shown in **Figure 2**, a transient current is generated when different potentials are applied to the electrodes, which results from the double-layer charging. However, the current presents different changes with prolonging the time at different potentials. The current is rapidly decreased by increasing the time and finally goes to zero when the potential is –0.60 V, indicating that almost no $Co(OH)_2$ nucleates and grows on the electrode. This is consistent with the result obtained in the CV tests. When the applied potential is reduced to –0.65 V, the current is decreased to –2.55 mA in a short time of about 15 s, then rises rapidly and tends to a stable value of about –3.95 mA after 600 s. The rapid rise in the current is mainly related to the significant increase in the electrode surface area resulting from the nucleation and growth of the $Co(OH)_2$. Therefore, the short time (about 15 s) can be defined as the nucleation incubation period. Accompanied by the continuous growth of the nuclei, they may be connected with each other, resulting in the formation of deposits with a comparatively stable surface morphology. Correspondingly, the current begins to stabilize after reaching a maximum value of about –4.4 mA, meaning that $Co(OH)_2$ is deposited on the electrode surface at a constant rate. The change in current with time at –0.70 V is very similar to that at –0.65 V. Only two subtle differences are observed, corresponding to a shorter nucleation incubation period (11 s) and a higher deposition rate. The phenomenon is attributed to the increase in the driving force for the nucleation and growth of $Co(OH)_2$ when the potential is increased from –0.65 V to –0.70 V. When the potential is further increased to –0.80 V and –0.95 V, the nucleation incubation period almost disappears, indicating that the nucleation is almost instantaneous. The current presents a significant decline trend after it reaches a maximum value, which is significantly deviated from the change trend presented in the curves obtained at –0.65 V and –0.70 V. It can be concluded that the electrode reactions are gradually controlled by the diffusion of the active ions. When a high potential is exerted on the electrode, a large number of active ions around the electrode are violently consumed for the nucleation and growth of $Co(OH)_2$, resulting in active ions poor after about 300 s. The diffusion of ions towards the electrode surface gradually becomes the rate-controlling step of the electrode reactions. When the diffused ions cannot timely compensate for those consumed by the reactions, the current is gradually decreased with the time. Comparatively speaking, the decline trend is prominent at –0.95 V due to more serious consumption of the active ions at a high potential.

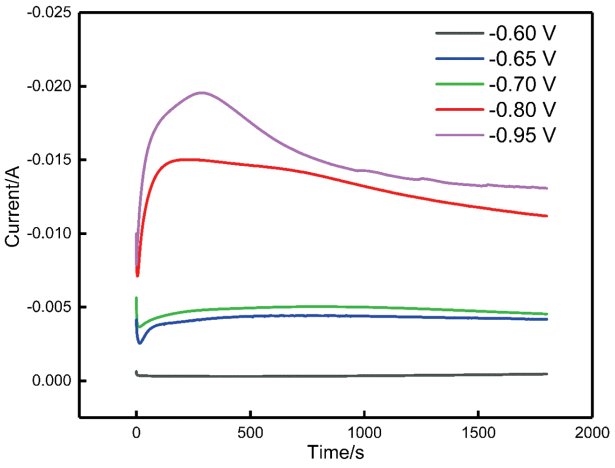

Figure 2: Chrono-amperograms recorded on nickel foam in a solution consisting of 0.1 mol·L^{-1} $Co(NO_3)_2$

Instantaneous nucleation and progressive nucleation are two important nucleation processes. In the instantaneous nucleation process, the nuclei are formed almost simultaneously. The growth of the nuclei will be predominant during the subsequent deposition. In the progressive nucleation process, the formed nuclei grow during the deposition, accompanied with which the new nuclei are constantly formed on the substrate surface or the deposit surface. The crystallinity of the deposit obtained by instantaneous nucleation is higher than that by continuous nucleation.[24] Hills has derived two equations describing the relationship between current and time to determine the nucleation process on the electrode surface.

For instantaneous nucleation:

$$I(t) = \frac{zFN_0\pi(2DC)^{3/2}M^{1/2}}{\rho^{1/2}}(t)^{1/2} \quad (3)$$

For progressive nucleation:

$$I(t) = \frac{2zFK_nN_0\pi(2DC)^{3/2}M^{1/2}}{\rho^{1/2}}(t)^{3/2} \quad (4)$$

where z is the valence number, N_0 is the initial nucleation number, D is the diffusion coefficient for the deposited ions (cm^2·s^{-1}), C is the bulk concentration of the deposited ions (mol·cm^{-3}), M is the atomic weight of the deposits (g·mol^{-1}), ρ is the density of the deposits (g·cm^{-3}), K_n is the nucleation constant, I(t) is the corresponding current when time is t (A), and t is the polarization time (s).

The above equations show that the current is linear with $t^{1/2}$ and $t^{3/2}$, respectively, when the $Co(OH)_2$ is

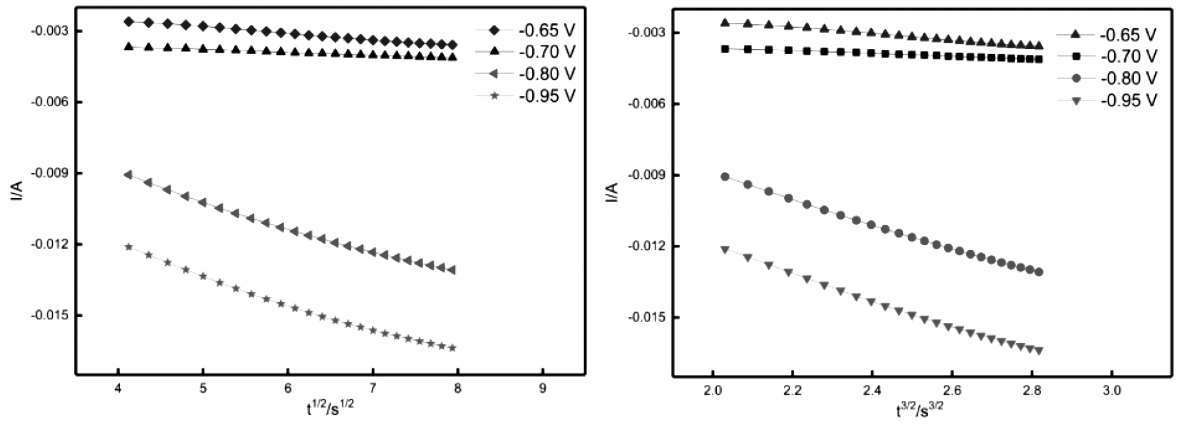

Figure 3: I as a function of $t^{1/2}$ and $t^{3/2}$ at various potentials ranging from –0.65 V to –0.95 V

formed by the instantaneous nucleation mode and the progressive nucleation mode. The experimental data from the rising portion in **Figure 2** were collected to investigate the nucleation mechanism. As shown in **Figure 3**, I is in a good linear relation with $t^{1/2}$ and $t^{3/2}$. Owing to some parameters (such as N_0 and D) in Eqations (3) and (4) cannot be determined precisely, the theoretical curve cannot also be drawn clearly. Therefore, the nucleation mechanism is difficult to be determined accurately by comparing the theoretical curves and experimental curves.

The other model deduced by Scharifker-Hills can solve the problem mentioned above due to some parameters crossed out efficiently by normalizing I and t to the peak current I_m and the corresponding peak time t_m.

For instantaneous nucleation:

$$\left(\frac{I}{I_m}\right)=\frac{1.9542}{t/t_m}\left\{1-\exp[-1.2564(t/t_m)]\right\}^2 \qquad (5)$$

For progressive nucleation:

$$\left(\frac{I}{I_m}\right)=\frac{1.2254}{t/t_m}\left\{1-\exp[-2.3367(t/t_m)^2]\right\}^2 \qquad (6)$$

There is a very short nucleation period (t_0) observed in **Figure 2**. Prior to the nucleation, which can interfere with the theoretical curve. Therefore, t and t_m are represented by $t' = t - t_0$ and $t_m' = t_m - t_0$ in order to obtain the correct normalization curve. The $(I/I_m)^2 - t/t_m$ curves obtained at different potentials and two theoretical curves are plotted and compared (**Figure 4**). Comparatively speaking, the experimental fitting curves better coincide with the theoretical curve of instantaneous nucleation. It can be concluded that the instantaneous nucleation dominates the deposition of $Co(OH)_2$.

3.2 Morphological evolution of $Co(OH)_2$ with potentials and $Co(NO_3)_2$ concentrations

The morphologies of the deposits are observed by SEM to reveal the effect of deposition potential and concentration on the morphological evolution. **Figure 5a** to **5c** presents the morphologies of the deposits prepared at the applied potentials of –0.60 V, –0.65 V, –0.95 V in the solution with 0.1 mol·L^{-1} $Co(NO_3)_2$. It can be found that their surface morphology changes significantly with the deposition potential. When a potential of –0.60 V is applied, there are almost no deposits adhering to the nickel foam surface due to initial grains and boundaries clearly observed. It indicates that –0.6 V is insufficient to drive the nucleation and growth of $Co(OH)_2$, which is completely in accordance with the result obtained in CV. When the potential moves to a more negative value of –0.65 V, the surface of the nickel foam is obviously covered with a thin layer of deposits with a honeycomb-like porous structure. The deposition rate is further enhanced at a higher potential of –0.95 V, resulting in an obvious increase in the thickness of the deposit. However, some gaps with a width of 5 ìm can be clearly observed. The above result demonstrates that a high potential can accelerate the deposition; however, it can also deteriorate the quality of the deposit. When the $Co(NO_3)_2$ concentration is evaluated to 0.9 mol·L^{-1}, the deposit can be obtained on the nickel foam surface at the applied potential of –0.60 V (**Figure 5a**), the morphology of which is very similar to that at –0.65 V in 0.1 mol·L^{-1} $Co(NO_3)_2$ solution. Some fine cracks are formed on the deposit surface when the potential reaches

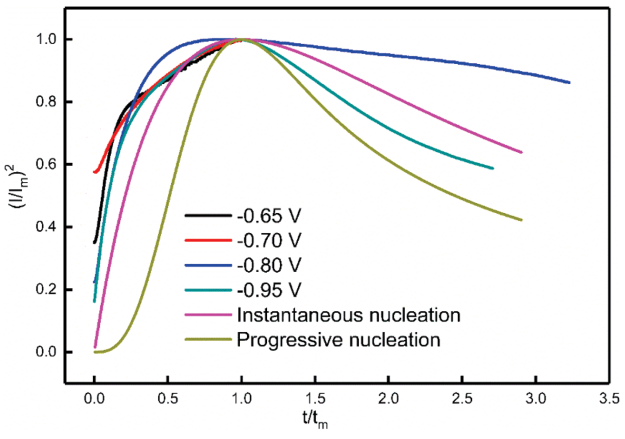

Figure 4: Experimental and theoretical curves between $(I/I_m)^2$ and t/t_m

–0.65 V (**Figure 5b**). Moreover, some coarse particles of the deposit protrude out of the surface due to the overgrowth of the partial zones. Those particles cluster to form coarser particles with irregular shape, which are mainly distributed around the edge of the limbs of the nickel foam. This should be attributed to the edge effect. With further increasing the potential to –0.95 V, the deposit becomes denser and thicker, and tiny cracks are also transformed into coarse gaps **(Figure 5c)**.

SEM images with a higher magnification are obtained to present more morphological characteristics of the deposits (**Figure 6**). No deposited layer was obviously formed at –0.60 V when the $Co(NO_3)_2$ concentration is 0.1 mol·L^{-1}, besides a small amount of suspected deposits particles (**Figure 6a**). A layer of loose and porous deposits completely covers the surface of nickel foam at –0.65 V (**Figure 6b**). The image located at the right left corner of the figure clearly reveals that the irregular petal-like nanosheets with a thickness of about 25.6 nm, preferentially grow on the comparatively leveled surface of the deposit, which connect with each other to form the honeycomb-like structure. When the potential of –0.95 V is applied, a stronger driving force accelerates the growth of these nanosheets in three-dimensional directions (**Figure 6c**). Moreover, new nanosheets grow up on the flat surface of the deposit, resulting in the surface split into many fine pores with a smaller size. The layer also becomes more compact due to the growth and interconnection among the numerous nanosheets, which may cause the reduction in specific surface area of the deposit. It is clear that $Co(OH)_2$ can be deposited at a very low potential (–0.60 V) in a high concentration solution (**Figure 6a**); however, it is hardly visible in –0.60 V in a low concentration solution (**Figure 6a**). The morphology in the majority of deposited surface is very similar to that shown in **Figure 6b**. Comparatively speaking, the former is compacter than the latter. Moreover, a considerable number of fine/coarse flower-like particles with size from 0.27 to 2.7 μm protrude in local areas of the deposit surface. With further increasing the potential to –0.65 and –0.95 V, more and more nanosheets cluster together and form a compact deposit. Especially at –0.95 V, the volume fraction of pores in the deposit layer is greatly reduced. It is proved that a high potential efficiently promotes the growth of nanosheets; however, it is not beneficial to the increase in specific surface area due to the overgrowth of nanosheets. Based on the morphological evolution, it is easy to deduce that the deposit with the maximum specific surface area can be synthesized at a suitable combination of potential (–0.65 V) and $Co(NO_3)_2$ concentration (0.1 mol·L^{-1}).

The morphological evolution of the deposit can be intuitively described as followed. Many nuclei are formed instantaneously by the instantaneous nucleation mode. Accompanied with the growth of those nuclei, the grain boundaries are formed and crosslinked around the grains, resulting in the formation of a thin deposited layer. Then the growth of the grains is inhibited along the two-dimensional direction parallel to the nickel foam surface, the vertical growth becomes dominant. The grain boundary with high energy grows preferentially with the prolonged time when compared with the grains. Some irregular nano-walls sprout along the grain boundaries, which separate the deposit surface into numerous grids with different sizes. Nano-walls gradually grow

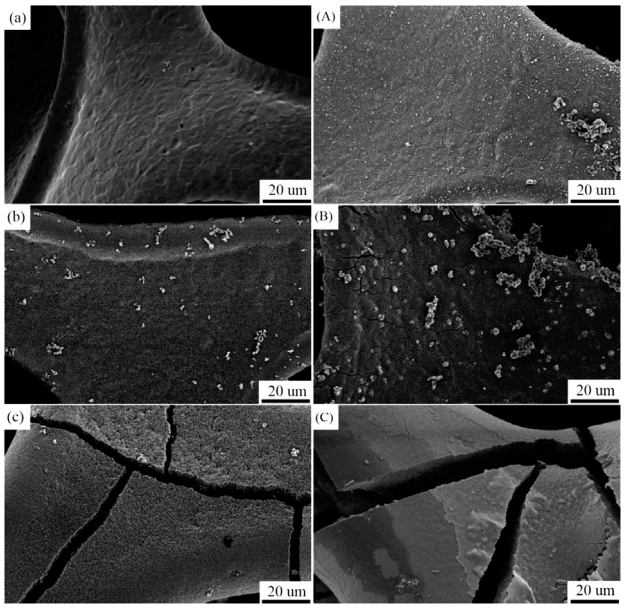

Figure 5: Low-magnification SEM images of the deposits prepared at different potentials and $Co(NO_3)_2$ concentrations: a) –0.60 V 0.1 mol·L^{-1}, b) –0.65 V 0.1 mol·L^{-1}, c) –0.95 V 0.1 mol·L^{-1}

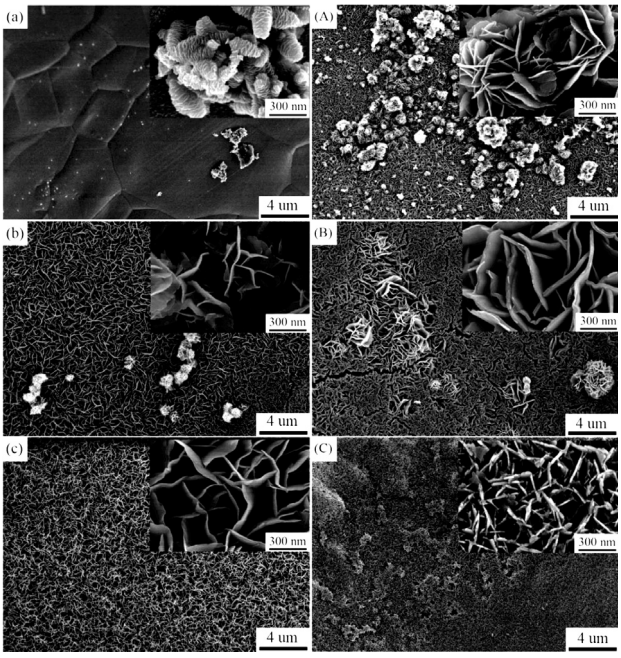

Figure 6: High-magnification SEM images of deposits prepared at different deposition potentials and $Co(NO_3)_2$ concentrations: a) –0.60 V 0.1 mol·L^{-1}, b) –0.65 V, 0.1 mol·L^{-1}, c) –0.95 V 0.1 mol·L^{-1}, A) –0.60 V 0.9 mol·L^{-1}, B) –0.65 V 0.9 mol·L^{-1}, C) –0.95 V 0.9 mol·L^{-1}

into nanosheets, which protrude into the solution. Due to the weak conductivity of $Co(OH)_2$, the resistance between the protruding nanosheets and the substrate will be gradually increased, the growth of nanosheets are correspondingly slowed down. When a stronger driving force is applied resulting from a higher potential or a higher $Co(NO_3)_2$ concentration, a portion of zones with high growing rate on the flat surface of deposit can protrude out of the surface and grow into some fine particles. Those particles may grow and connect into new nano-walls, which will be transformed into new nanosheets. Moreover, some new growth sites may be formed resulting from the interconnection of nanosheets, which further grow into fine or coarse flower-like particles. Correspondingly, a compacter deposit layer is formed.

3.3 Electrochemical performance

Figure 7 shows cyclic voltametry (CV) curves of $Co(OH)_2$/NF prepared in the (0.1, 0.5, 0.7 and 0.9) mol·L^{-1} $Co(NO_3)_2$ solutions with different potentials, which are recorded at a scanning rate of 5 mV·s^{-1} in a 2 mol·L^{-1} KOH solution. It is clear that the CV profiles are significantly deviated from the ideal rectangular shape. Moreover, two redox peaks can also be observed, indicating that the electrodes exhibit typical pseudocapacitance behavior, namely the capacitance mainly originates from the oxidation/reduction reactions. For the first redox peak (**Figure 7a**), the oxidation peak is located at 0.025 V, and the corresponding reduction peak can be observed at –0.045 V. Two reactions are followed:

$$Co(OH)_2 + OH^- e^- \rightarrow CoOOH + H_2O \quad \text{(Oxidation reaction)} \tag{7}$$

$$CoOOH + H_2O + e^- \rightarrow Co(OH)_2 + OH^- \quad \text{(Reduction reaction)} \tag{8}$$

For the second redox peak, the oxidation and reduction peaks are formed at 0.24 V and 0.175 V, respectively. The corresponding reactions are followed:

$$CoOOH + OH^- e^- \rightarrow CoO_2 + H^2O \quad \text{(Oxidation reaction)} \tag{9}$$

$$CoO_2 + H_2O + e^- \rightarrow CoOOH + OH^- \quad \text{(Reduction reaction)} \tag{10}$$

The whole reaction process can be clearly described throughout the sweeping. When the potential reached to 0.025 V, the $Co(OH)_2$ deposited on the nickel will be transformed to CoOOH. Along with the increase to 0.24 V in potential, CoOOH is further oxidized into CoO_2. During the reverse sweeping, CoO_2 is reduced into CoOOH and $Co(OH)_2$. Both $Co(OH)_2$ and CoOOH have the same cobalt structure and large interlayer spacing, which is very beneficial for H^+ to intercalation and deintercalation during the charge-discharge.[13] As a result, the cycling performance and stability of the $Co(OH)_2$/NF electrode can be improved. The result was verified by research.[25,26] **Figure 7b** clear inspection reveals that the integrated area of CV profiles present the incline tendency with increasing the potential in the (0.1, 0.5, 0.7 and 0.9) mol·L^{-1} $Co(NO_3)_2$ solutions, meaning that the high deposited potential does not favor to the improvement in capacitance of the electrodes. Besides the potential, the increase in $Co(NO_3)_2$ concentration is not also beneficial to the enhancement in capacitance due to the integrated area of CV profile in 0.1 mol·L^{-1} $Co(NO_3)_2$ solution larger than that in (0.5, 0.7 and 0.9) mol·L^{-1} $Co(NO_3)_2$ solution at any given deposited potential. The specific capacitance is a very important index characterizing the power storage capacity in a unit mass of active substances, which is related not only to the capacitance, but also to the mass. The effect of potential and $Co(NO_3)_2$ concentration on the mass of the deposited substances is investigated. It is clear that more substances can be deposited in a high-concentration $Co(OH)_2$ solution at a given potential. Considering the changes in the mass of deposits and the integrated area of CV curves with potential and $Co(NO_3)_2$ concentration, it is easy to draw a conclusion that the high specific capacitance can be obtained in an electrode prepared in a low $Co(NO_3)_2$ concentration solution with a low applied potential.

b) different concentration of $Co(NO_3)_2$ solution

The specific capacitance of the $Co(OH)_2$ can be calculated according to the following equation:

$$C_m = \frac{\int i dV}{2 \times S \times \Delta V \times m} \tag{11}$$

where C_m (F·g^{-1}) is the specific capacitance measured from CV tests, $\int i dV$ is the integrated area of the CV curves, DV (V) represents the potential drop during discharge, S (V·s^{-1}) is the scan rate and m (mg) is the mass of the active material on the electrode.

The calculated results are shown in **Table 1**. The specific capacitance reaches 836 F·g^{-1} for $Co(OH)_2$ deposited at –0.65 V in a 0.1 mol·L^{-1} $Co(NO_3)_2$ solution. The value is gradually decreased by applying the more negative potential, finally is reduced to 496 F·g^{-1} at –0.95 V (only about 59.3 % that at –0.65 V). When the concentration is increased to 0.9 mol·L^{-1}, a similar phenomenon is also observed. The value of $Co(OH)_2$ deposited at –0.95 V is only about 44.4 % that at –0.60 V. Moreover, the specific capacitance value of $Co(OH)_2$ deposited in the 0.9 mol·L^{-1} $Co(NO_3)_2$ solution is 62.1–80.9 % that in the 0.1 mol·L^{-1} $Co(NO_3)_2$ solution at the same potential, which is well in accordance with the above analyses.

The galvanostatic charge/discharge tests were also applied to calculate the specific capacitance of $Co(OH)_2$ (**Figure 9**). The specific capacitance can be calculated by the following Equation (12):

$$C_m = \frac{i\Delta t}{\Delta V \times m} \tag{12}$$

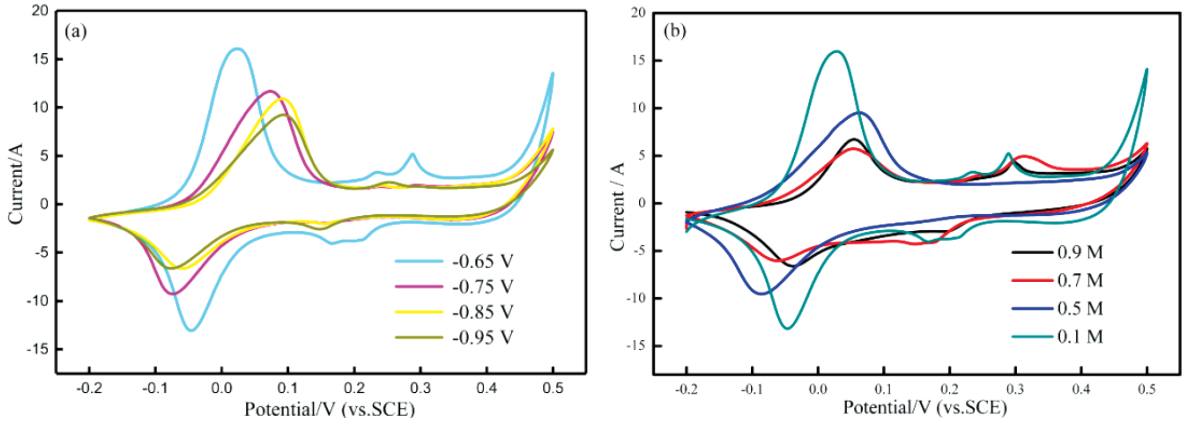

Figure 7: Cyclic voltammetry (CV) curves recorded on the $Co(OH)_2$/NF electrodes at a scanning rate of 5 $mV \cdot s^{-1}$. a) 0.1 $mol \cdot L^{-1}$ $Co(NO_3)_2$ solution, b) different concentration of $Co(NO_3)_2$ solution

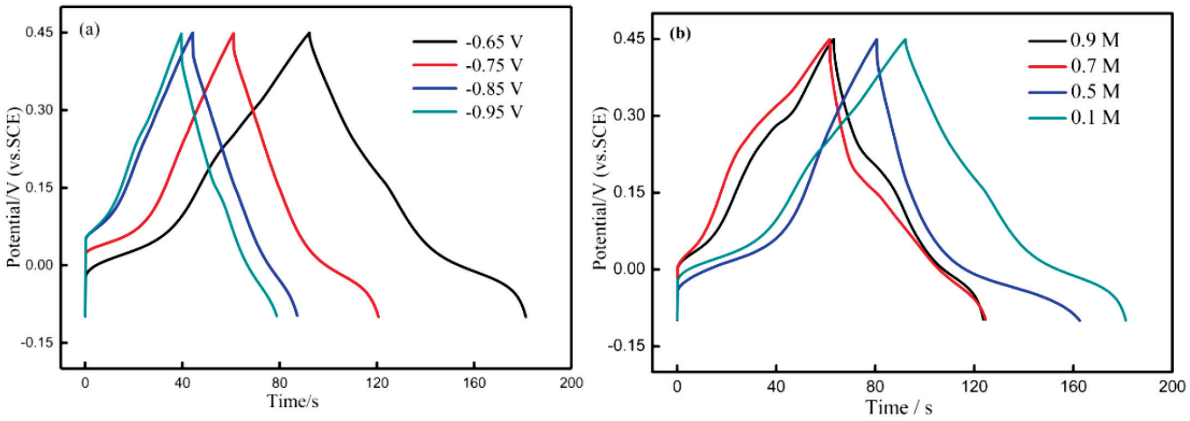

Figure 8: Galvanostatic charge/discharge curves recorded on the $Co(OH)_2$/NF electrodes at a current density of 4 $A \cdot g^{-1}$:a) 0.1 $mol \cdot L^{-1}$ $Co(NO_3)_2$ solution

where I is the applied constant current (A), m is the mass of $Co(OH)_2$, ÄV is the potential window during cycling and Δt is the time of the cycle (s).

The results are shown in **Table 1**, which present the completely same change with $Co(NO_3)_2$ concentration and applied potential. The specific capacitance is reduced from 725 $F \cdot g^{-1}$ to 315 $F \cdot g^{-1}$ with decreasing the potential from –0.65 V to –0.95 V for $Co(OH)_2$ deposited in the 0.1 $mol \cdot L^{-1}$ $Co(NO_3)_2$ solution. The value is only drastically reduced from 567 $F \cdot g^{-1}$ to 130 $F \cdot g^{-1}$ when the potential is decreased from –0.60 V to –0.95 V for $Co(OH)_2$ deposited in the 0.9 $mol \cdot L^{-1}$ $Co(NO_3)_2$ solution. The value is reduced about 32–59 % for $Co(OH)_2$ deposited in the 0.1 $mol \cdot L^{-1}$ $Co(NO_3)_2$ solution when compared that in the 0.9 $mol \cdot L^{-1}$ $Co(NO_3)_2$ solution.

The change in specific capacitance of the electrodes prepared at different potentials in the solutions with different concentrations of $Co(NO_3)_2$ is closely related to the evolution in the morphology of the deposits. As analyzed above, the overgrowth of the deposits resulting from a high concentration $Co(NO_3)_2$ and a high applied potential will significantly reduce their specific area, which means that the unit mass of deposits with less active sites can undergo insufficient and incomplete redox reactions, and provide fewer tunnels and a stronger resistance to the transportation of ions and electrons. Subsequently, the improvement in the potential and $Co(NO_3)_2$ concentration does not contribute to the improvement in the specific capacitance.

Table 1: Specific capacitance measured by CV and galvanostatic charge/discharge tests

Concentration	Potential	CV	Galvanostatic charge/discharge
0.1 $mol \cdot L^{-1}$	–0.65 V	836 $F \cdot g^{-1}$	725 $F \cdot g^{-1}$
	–0.75 V	742 $F \cdot g^{-1}$	482 $F \cdot g^{-1}$
	–0.85 V	523 $F \cdot g^{-1}$	349 $F \cdot g^{-1}$
	–0.95 V	496 $F \cdot g^{-1}$	315 $F \cdot g^{-1}$
0.9 $mol \cdot L^{-1}$	–0.60 V	694 $F \cdot g^{-1}$	567 $F \cdot g^{-1}$
	–0.65 V	593 $F \cdot g^{-1}$	494 $F \cdot g^{-1}$
	–0.75 V	509 $F \cdot g^{-1}$	326 $F \cdot g^{-1}$
	–0.85 V	423 $F \cdot g^{-1}$	221 $F \cdot g^{-1}$
	–0.95 V	308 $F \cdot g^{-1}$	130 $F \cdot g^{-1}$

The cycle stability is another important parameter evaluating the electrochemical performance of the supercapacitors, which is used to characterize the performance attenuation of continuous charge and discharge under the same condition. The cycle stability of the $Co(OH)_2$/NF

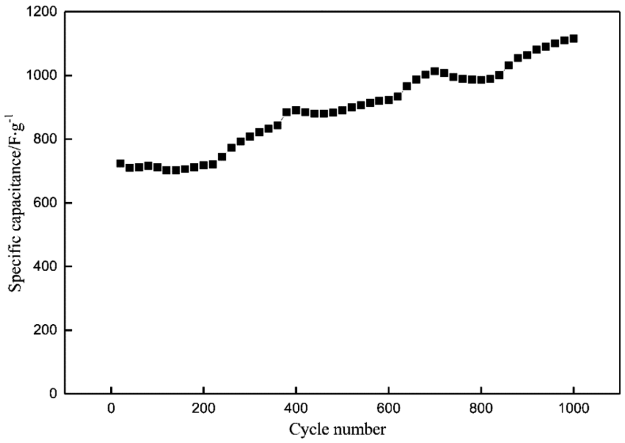

Figure 9: Cyclic performance of the $Co(OH)_2$/NF electrode at a scanning rate of 5 $mV \cdot s^{-1}$ for 1000 cycles

electrode was examined in 2 $mol \cdot L^{-1}$ KOH electrolyte at a scanning rate of 5 $mV \cdot s^{-1}$. As shown in **Figure 9**, the specific capacitance presents the gradual rising tendency with the increase in the cycle number, and a high value of 1116 $F \cdot g^{-1}$ (133.65 % of initial value) is finally retained after 1000 cycles, which indicates that the electrode presents an excellent capacity retention and is not subject to a serious degradation during the repetitive and continuous charge and discharge. The phenomenon about the increase in specific capacitance with prolonging the cycle time has been reported previously for other electrodes. Z. P. Feng et al.[27] synthesized MnO_2 multilayer nanosheets clusters were prepared via electrochemical deposition route, which has about 133 % increase in the specific capacitance after 1000 cycles. X. H. Lu[28] et al.[30] synthesized large-area manganese oxide nanorod arrays (MONRAs) and herringbones (MOHBs) on F-doped SnO_2 coated glass (FTO) substrates by a electrochemical method. The specific capacitance from 411.4 $F \cdot g^{-1}$ to 507 $F \cdot g^{-1}$ after 1500 cycles. Z. Gao et al.[29] synthesized neighboring sheets separate graphene nanosheet/ Ni^{2+}/Al^{3+} layered double-hydroxide (GNS/LDH) composite for supercapacitor material by a hydrothermal method. The composite exhibits a maximum specific capacitance of 781.5 $F \cdot g^{-1}$ and an excellent cycle life with an increase of the specific capacitance of 38.07 % after 50 cycle tests. Even after 200 cycle tests, the increase of the capacitance is 22.56 % compared with the initial capacitance. M. J. Pang et al.[30] prepared the porous structures mixed-phase CoO/Co_3O_4 nanocomposites by a facile ethanol-assisted solvothermal approach. The CoO/Co_3O_4 electrode exhibits a high capacitance of 451 $F \cdot g^{-1}$ at a current density of 1 $A \cdot g^{-1}$ and superior cycle stability (108 % retention after 5000 cycles). According to previous researches,[27–33] the phenomenon of increasing the specific capacitance is mainly attributed to more active sites in the active substance activated during the cycle. Besides that, further elaboration of its mechanism in this study, the structural transformation may be the other essential factor causing the significant rising in the specific capacitance in this study, which is validated by comparing the difference in morphology and structure of the deposited active substances before and after long-term cycling.

Figure 10 demonstrates SEM images of the active substances deposited in the 0.1 $mol \cdot L^{-1}$ $Co(NO_3)_2$ solution with the applied potential of –0.65 V before and after the electrochemical tests (1000 cycles). The deposits are composed of many nanosheets prior to the electrochemical tests (**Figure 10a**). Some anisotropic nanosheets cluster together to form the interlaced follower-like morphology. The other approximately parallel nanosheets form the loose platelets. After the electrochemical tests, the drastic change in morphology can be clearly observed (**Figure 10b**). The loose stacked fine sheets are transformed into the dense coarse sheets. Clearly observation reveals that those are composed of several fine sheets, among which tiny gaps remained. The morphological evolution indicates that the KOH electrolyte can accelerate the cluster of nanosheets by compressing the space among them, which is closely associated with the removal of nitrates incorporated into nanosheets. **Figure 11** indicates a narrow spectral scan of the Co element performed on the substances prepared

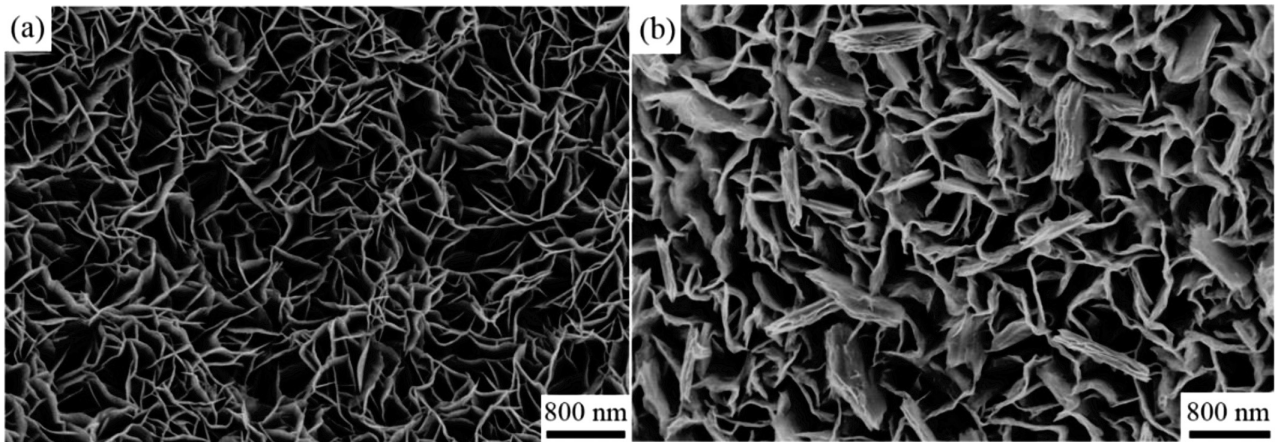

Figure 10: SEM images of the deposits: a) before and b) after the cycle testing

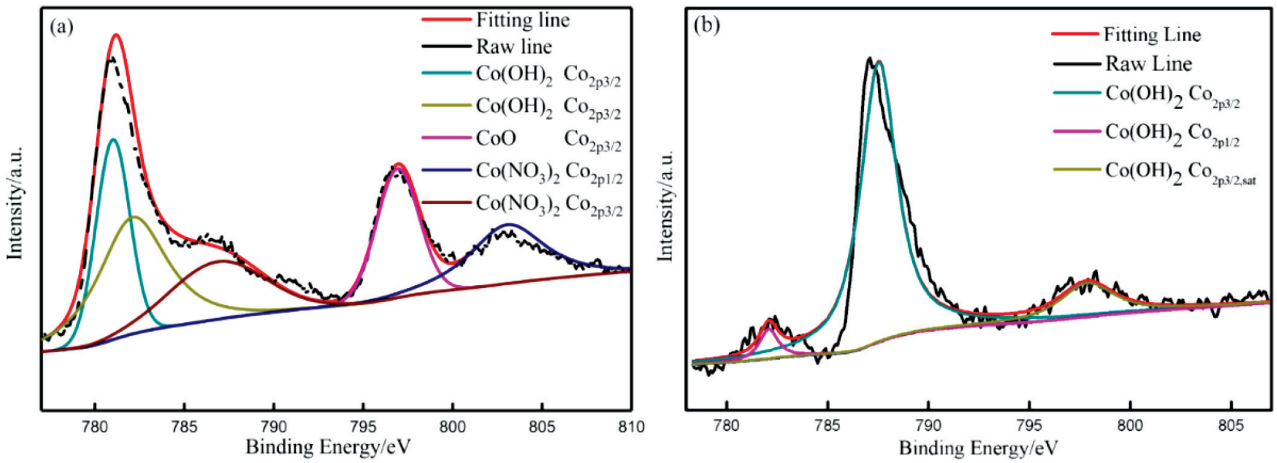

Figure 11: XPS spectra of Co in the deposits: a) before and b) after the cycle testing

in the 0.1 mol·L^{-1} $Co(NO_3)_2$ solution with the applied potential of –0.65 V before and after the electrochemical tests, which can be used to identify the chemical valence states of Co. Prior to the electrochemical tests, two strong peaks located at 781.00 eV and 796.5 eV can be clearly observed (**Figure 11a**). The strongest peak is in good agreement with that of Co^{2+} in $Co(OH)_2$ and the other coincides with that of Co^{2+} in CoO. A small amount of $Co(NO_3)_2$ can be confirmed due to the two peaks related to Co^{2+} in $Co(NO_3)_2$ with comparatively low intensities at 786.850 eV and 803.05 eV, which are incorporated into the $Co(OH)_2$ during the synthesis. It is clear that the deposited substances are mainly composed of $Co(OH)_2$, accompanied with a small amount of CoO and $Co(NO_3)_2$. Among them, only $Co(OH)_2$ and CoO are responsible for the charge storage by participating in the redox reactions occurring on the electrode surface. The incorporated $Co(NO_3)_2$ into the active substances seriously reduces the efficient active sites and deteriorates the electrochemical performance. However, the XPS result indicates that $Co(NO_3)_2$ incorporated into the nanosheets has been removed completely after the electrochemical tests (**Figure 11b**). It can be concluded that OH^- will infiltrate into the tiny gaps among the sheets and contacts with the nanosheets sufficiently when the electrode is immersed into the KOH electrolyte for the electrochemical tests, which will result in the removal of the interlayer nitrates. Similar results were reported in previous studies.[13] The removal of nitrates can be regarded as an essential factor causing the improvement in specific capacitance due to the increase in active sites. The other factor may be associated with the structural change of active substances. **Figure 12a** shows the high-resolution TEM image of the as-prepared deposits in the 0.1 mol·L^{-1} $Co(NO_3)_2$ solution with the applied potential of –0.65 V. It is clear that the synthesized deposit possesses poor crystallinity due to its disordered lattice fringe, which can be identified as a-$Co(OH)_2$, as reported in the other investigations.[13,22,34,35] The transformation in phase constituent should occur when the deposit is subject to the electrochemical tests owing to an ordered lattice fringe observed clearly (**Figure 12b**). A d-spacing of 0.237 nm is indexed, which is in accordance with that of b-$Co(OH)_2$ (JCPDS

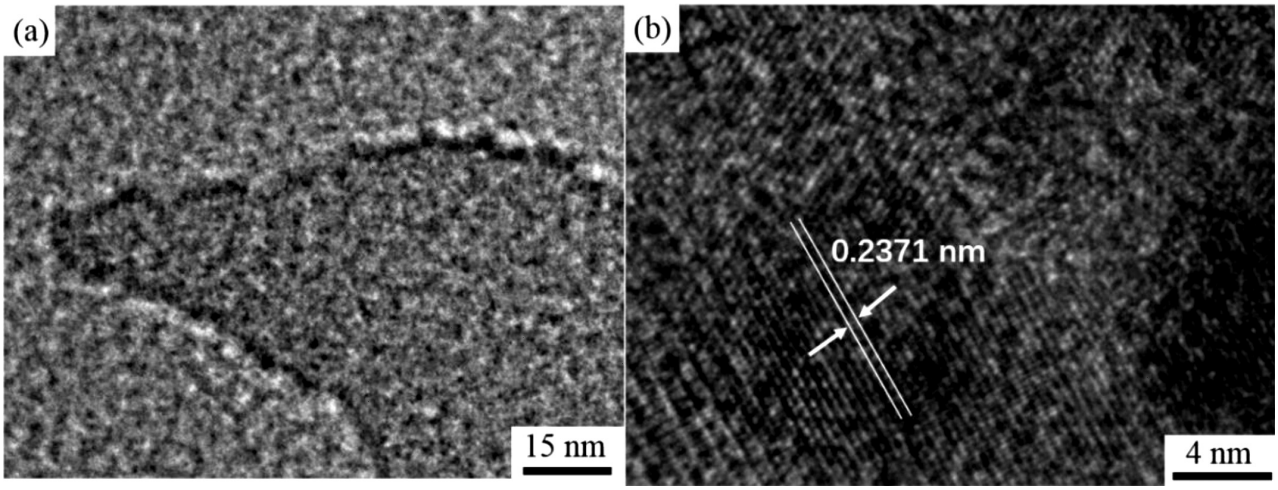

Figure 12: HRTEM images of the deposits: a) before and b) after the cycle testing

card No.30–0443). Compared with the disorder α-$Co(OH)_2$, the order β-$Co(OH)_2$ exhibits better conductivity, which will enhance the specific capacitance of the electrode.[36] Based on the analyses above, the improvement in specific capacitance after 1000 cycles can attributed to an increase in the active sites and the transformation of á-$Co(OH)_2$ into b-$Co(OH)_2$. T. Deng et al.[13] also found that OH^- like a scalpel removed NO_3^- from α-$Co(OH)_2$ and transformed α-$Co(OH)_2$ into β-$Co(OH)_2$. The change made the specific capacitance retain 95.7 % of its initial value (800 $F \cdot g^{-1}$ at the current of 2 $A \cdot g^{-1}$) after 8000 cycles.

4 CONCLUSIONS

1) $Co(OH)_2$ nanosheets were electrodeposited on nickel foam by the two reactions including an electrochemical reaction $NO_3^- + 7H_2O + 8e^- \rightarrow NH_4^+ + 10OH^-$ occuring at about –0.6 V (vs. SCE) and a following chemical reaction $Co_2^+ + 2OH^- \rightarrow Co(OH)_2$. $Co^{2+} + 2OH^- \rightarrow Co(OH)$ $2Co(OH)_2$ nuclei were formed by instantaneous nucleation.

2) The deposited potential and $Co(NO_3)_2$ concentration produced significant effects on the morphologies of $Co(OH)_2$. With the increase in potential and $Co(NO_3)_2$ concentration, the deposits became more compact and possessed the lower specific area due to their overgrowth. The deposit with the highest specific area was obtained at the potential of –0.65 V in the 0.1 $mol \cdot L^{-1}$ $Co(NO_3)_2$ solution.

3) The specific capacitance of the $Co(OH)_2$/NF prepared in the 0.1 $mol \cdot L^{-1}$/0.9 $mol \cdot L^{-1}$ $Co(NO_3)_2$ solution presented a reduction tendency with an increase in the potential. The value of the electrode prepared in the 0.1 $mol \cdot L^{-1}$ $Co(NO_3)_2$ solution was higher than that in the 0.1 $mol \cdot L^{-1}$ $Co(NO_3)_2$ solution. The highest value was obtained in the electrode prepared at the potential of –0.65 V in the 0.1 $mol \cdot L^{-1}$ $Co(NO_3)_2$ solution, which was 836 $F \cdot g^{-1}$ in CV tests and 725 $F \cdot g^{-1}$ in galvanostatic charge/discharge tests.

4) The electrode prepared at the potential of –0.65 V in the 0.1 $mol \cdot L^{-1}$ $Co(NO_3)_2$ solution also exhibited the excellent cyclic stability with 133.65 % of initial capacity retained after 1000 cycles. The activation of more active sites resulting from the removal of incorporated $Co(NO_3)_2$ into the active substances and the transformation of a-$Co(OH)_2$ into b-$Co(OH)_2$ with high conductivity were responsible for the change.

Acknowledgment

This work was financially supported by the National Natural Science Foundation of China, China (51471105), "Shu Guang" project of Shanghai Municipal Education Commission and Shanghai Education Development Foundation (12SG44).

5 REFERENCES

[1] G. P. Wang, L. Zhang, J. J. Zhang, A Review of Electrode Materials for Electrochemical Super-capacitors, Chem. Soc. Re., 41 (**2012**) 797–828, doi:10.1039/c1cs15060j

[2] T. Yan, R. Y. Li, L. Zhou, C. Y. Ma, Z. J. Li, Three-dimensional electrode of Ni/Co layered double hydroxides@$NiCo_2S_4$@graphene@Ni foam for supercapacitors with outstanding electrochemical performance, Electrochimica Acta., 176 (**2015**) 1153–1164, doi:10.1016/J.electacta.(**2015**).07.160

[3] T. Deng, Y. Lu, W. Zhang, M. L. Sui, X. Y. Shi, D. Wang, W. T. Zheng, Inverted design for high-performance supercapacitor via $Co(OH)_2$-derived highly-oriented MOF electrodes, Adv. Energy Mater., 8 (**2017**) 1870030, doi:10.1002/aenm.201702294

[4] L. B. Kong, M. Liu, J. W. Lang, Y. C. Luo, L. Kang, Asymmetric supercapacitor based on loose-packed cobalt hydroxide nanoflake materials and activated carbon, J. Electrochem. Soc., 156 (**2009**) A1000–A1004, doi:10.1149/1.3372528

[5] T. Xue, X. Wang, J. M. Lee, Dual-template synthesis of $Co(OH)_2$ with mesoporous nanowire structure and its application in supercapacitor, J. Power Sources, 201 (**2012**) 382–386, doi:10.1016/j.jpowsour.2011.10.138

[6] Y. F. Tang, Y. Y. Liu, S. X. Yu, S. C. Mu, S. H. Xiao, Y. F. Zhao, F. M. Gao, Morphology controlled synthesis of monodisperse cobalt hydroxide for supercapacitor with high performance and long cycle life, J. Power Sources, 256 (**2014**) 160–169, doi:10.1016/j.jpowsour.2014.01.064

[7] V. Pierre, M. Christine T. G. Christine, R. Guillaume, M. Herve, J. C. Dupin, E. Erik, L. Fabrice, High-performing monometallic cobalt layered double hydroxide supercapacitor with defined local structure, Adv. Funct. Mater., 24 (**2014**) 4831–4842, doi:10.1002/adfm.201400310

[8] B. G. Choi, M. Yang, S. C. Jung, K. G. Lee, J. G. Kim, H. Park, T. J. Park, S. B. Lee, Y. K. Han, Y. S. Huh, Enhanced pseudocapacitance of ionic liquid/cobalt hydroxide nanohybrids, Acs Nano, 7 (**2013**) 2453–2460, doi:10.1021/nn305750s

[9] X. L. Sun, Z. Q. Jiang, C. X. Li, Y. Y. Jiang, X. Y. Sun, X. N. Tian, L. J. Luo, X. G. Hao, Z. J. Jiang, Facile synthesis of Co_3O_4 with different morphologies loaded on amine modified graphene and their application in supercapacitors, J. Alloy. Compd., 685 (**2016**) 507–517, doi:10.1016/j.jallcom.2016.05.282

[10] K. Matsui, T. Kyotani, A. Tomita, Hydrothermal synthesis of single-crystal $Ni(OH)_2$ nanorods in a carbon-coated anodic alumina film, Adv. Mater., 14 (**2002**) 1216–1219, doi:10.1002/1521-4095(20020903)14:17<1216::aid-adma1216>3.0.co;2-a

[11] J. K. Chang, C. M. Wu, I. W. Sun, Nano-architectured $Co(OH)_2$ electrodes constructed using an easily-manipulated electrochemical protocol for high-performance energy storage applications, J. Mater. Chem., 20 (**2010**) 3729–3735, doi:10.1039/B925176F

[12] V. H. Nguyen, J. J. Shim, The 3D Co_3O_4/graphene/nickel foam electrode with enhanced electrochemical performance for supercapacitors, Mater. Lett., 139 (**2015**) 377–381, doi:10.1016/j.matlet.2014.10.128

[13] T. Deng, W. Zhang, O. Arcelus, J. G. Kim, J. Carrasco, S. J. Yoo, W. T. Zheng, J. F. Wang, H. W. Tian, H. B. Zhang, X. Q. Cui, T. Rojo, Atomic-level energy storage mechanism of cobalt hydroxide electrode for pseudocapacitors, Nat. Commun., 8 (**2017**) 1519, doi:10.1038/ncomms15194

[14] J. P. Cheng, M. Li, W. F. Zhang. J. S. Wu, F. Liu, X. B. Zhang, Evolution of cobalt hydroxide from 2D microplatelets to a 3D hierarchical structure mediated by precursor concentration3, RSC Advance., 3 (**2013**) 1330–1334, doi:10.1039/c3ra41351a

[15] Z. A. Hu, Y. L. Xie, Y. X. Wang, L. J. Xie, G. R. Fu, X. Q. Jin, Z. Y. Zhang, Y. Y. Yang H. Y. Wu, Synthesis of r-cobalt hydroxides with different intercalated anions and effects of intercalated anions on their morphology, basal plane spacing, and capacitive property, J. Phys. Chem. C., 113 (**2009**) 12502–12508, doi:10.1021/jp8106809

[16] C. M. Zhao, X. Wang, S. M. Wang, Y. Y. Wang, Y. X. Zhao, W. T. Zheng, Synthesis of $Co(OH)_2$/graphene/Ni foam nano-electrodes with excellent pseudocapacitive behavior and high cycling stability for supercapacitors, Int. J. Hydrogen Energ., 37 (**2012**) 11846–11852, doi:10.1016/j.ijhydene.2012.05.138

[17] M. Li, S. H. Xu, C. Cherry, Y. P. Zhu, R. Huang, R. J. Qi, P. X. Yang, L. W. Wang, P. K. Chu, Asymmetrical supercapacitor composed of thin $Co(OH)_2$ nanoflakes on three-dimensional Ni/Si microchannel plates with superior electrochemical performance, Electrochim. Acta, 149 (**2014**) 18–27, doi:10.1016/j.electacta.2014.10.091

[18] D. D. Zhao, W. J. Zhao, H. L. Li, Effects of deposition potential and anneal temperature on the hexagonal nanoporous nickel hydroxide films, Chem. Mater., 19 (**2007**) 3882–3891, doi:10.1021/cm062720w

[19] W. J. Zhou, J. Zhang, T. Xue, D. D. Zhao, H. L. Li, Electrodeposition of ordered mesoporous cobalt hydroxide film from lyotropic liquid crystal media for electrochemical capacitors, J. Chem. Mater., 18 (**2008**) 905–910, doi:10.1039/B715070A

[20] W. J. Zhou, M. W. Xu, D. D. Zhao, C. L. Xu, H. L. Li, Electrodeposition and characterization of ordered mesoporous cobalt hydroxide films on different substrates for supercapacitors, Micropor. Mesopor. Mat., 117 (**2009**) 55–60, doi:10.1016/j.micromeso.2008.06.004

[21] C. Xu, Z. H. Li, C. Yang, P. C. Zou, B. H. Xie, Z. Y. Lin, Z. X. Zhang, An ultralong, highly oriented nickel-nanowire-array electrode scaffold for high-performance compressible pseudocapacitors, Adv. Mater., 28 (**2016**) 4105–4110, doi:10.1002/adma.201505644

[22] K. M. Hercule, Q. L. Wei, A. M. Khan, Y. L. Zhao, X. C. Tian, L. Q. Mai, Synergistic rffect of hierarchical nanostructured MoO_2/$Co(OH)_2$ with largely enhanced pseudo capacitor cyclability, Nano Lett., 13 (**2013**) 5685–5691, doi:10.1021/nl403372n

[23] T. Zhao, H. Jiang, J. Ma, Surfactant-assisted electrochemical deposition of a-cobalt hydroxide for supercapacitors, J. Power Sources, 196 (**2011**) 860–864, doi:10.1016/j.jpowsour.2010.06.042

[24] H. Gomez, G. Riveros, D. Ramirez, R. Henriquez, R. Schrebler, R. Marotti, E. Dalchiele, Growth and characterization of ZnO nanowire arrays electrodeposited into anodic alumina templates in DMSO solution, J. Solid State Electr., 16 (**2012**) 197–204, doi:10.1007/s10008-011-1309-8

[25] J. Chen, F. Y. Cheng, Combination of lightweight elements and nanostructured materials for batteries, Accounts Chem. Res., 42 (**2009**) 713–723, doi:10.1021/ar800229g

[26] F. Y. Cheng, J. Liang, Z. L. Tao J. Chen, Functional materials for rechargeable batteries, Adv. Mater., 23 (**2011**) 1695–1715, doi:10.1002/adma.201003587

[27] Z. P. Feng, G. R. Li, J. H. Zhong, Z. L Wang Y. N. Ou, Y. X. Tong, MnO_2 multilnanosheet clusters evolved from monolayer nanosheets and their predominant electrochemical properties, Electrochem. Commun., 11 (**2009**) 706–710, doi:10.1016/j.elecom.2009.01.001

[28] X. H. Lu, D. Z. Zheng, T. Zhai, Z. Q. Liu, Y. Y. Huang, S. L. Xie, Y. X. Tong, Facile synthesis of large-area manganese oxide nanorod arrays as a high-performance electrochemical supercapacitor, Energ. Environ. Sci., 4 (**2011**) 2915–2921, doi:10.1039/c1ee01338f

[29] Z. Gao, J. Wang, Z. S. Li, W. L. Yang, B. Wang, M. J. Hou, Y He, Q. Liu, M. Tom, P. P. Yang, M. L. Zhang, L. H. Liu, Graphene nanosheet/Ni^{2+}/Al^{3+} layered double-hydroxide composite as a novel electrode for a supercapacitor, Chem. Mater., 23 (**2011**) 3509–3516, doi:10.1021/cm200975x

[30] M. J. Pang, G. H. Long, S. Jiang, Y. Ji, W. Han, B. Wang, X. L. Liu, Y. L. Xi, D. X. Wang, F. Z. Xu, Ethanol-assisted solvothermal synthesis of porous nanostructured cobalt oxides (CoO/Co_3O_4) for high-performance supercapacitors, Chem. Eng. J., 280 (**2015**) 377–384, doi:10.1016/j.cej.2015.06.053

[31] W. Y. Li, G. Li, J. Q. Sun, R. J. Zou, K. B. Xu, Y. G. Sun, Z. G. Chen, J. M. Yang, J. Q. Hu, Hierarchical heterostructures of MnO_2 nanosheets or nanorods grown on Au-coated Co_3O_4 porous nanowalls for high-performance pseudocapacitance, Nanoscale, 5 (**2013**) 2901-2908, doi:10.1039/C3NR34140B

[32] Y Dai, K. Wang, J. Xie, From spinel Mn_3O_4 to layered nanoarchitectures using electrochemical cycling and the distinctive pseudocapacitive behavior, Appl. Phys. Lett., 90 (**2007**) 104102, doi:10.1063/1.2711286

[33] A. Gaunand, W. L. Lim, From amorphous precipitates to sub-micronic crystalline platelets of $Co(OH)_2$: a kinetic study of the transformation process, Powder Technol., 128 (**2002**) 332–337, doi:10.1016/S0032-5910(02)00276-0

[34] Z. P. Liu, R. Z. Ma, M. Osada, K. Takada, T. Sasaki, Selective and controlled synthesis of r- and â-cobalt hydroxides in highly developed hexagonal platelets, J. AM. Chem. Soc., 127 (**2005**) 13869–13874, doi:10.1021/ja0523338

[35] A. A. M. Barmi, M. Aghazadeh, B. Arhami, H. M. Shiri, A. A. Fazl, E. Jangju, Porous cobalt hydroxide nanosheets with excellent supercapacitive behavior, Chem. Phys. Lett., 541 (**2012**) 65–69, doi:10.1016/j.cplett.2012.05.038

[36] M. Aghazadehn, S. Dalvand, M. Hosseinifard, Facile electrochemical Snthesis of uniform β-$Co(OH)_2$ nanoplates for higher performance supercapacitors, Ceram. Int., 40 (**2014**) 3485–3493, doi:10.1016/j.ceramint.2013.09.081